IS-PORTO 2023 PROCEEDINGS

Proceedings of the 8th International Symposium on DEFORMATION CHARACTERISTICS OF GEOMATERIALS Porto, 3rd - 6th September 2023

Discrete modelling of the mechanical response of Cuxhaven sand under shear and oedometric conditions using the rolling resistance contact model

Anjali Uday[1#], *Andrés Alfonso* Peña-Olarte[2], *Yuting* Wang[3]

[1,2,3] *Department of Civil, Geo and Environmental Engineering, Technical University of Munich, Germany*
[#]*Corresponding author: anjali.uday@tum.de*

ABSTRACT

The Distinct element method (DEM) is a promising approach to model the microscopic behaviour of granular materials, but the capability of the simulations to reproduce the mechanical response of real granular materials depends strongly on the contact model parameters utilized. The present study focuses on the calibration and validation of the rolling resistance linear model parameters for Cuxhaven sand based on the experimental results from triaxial and oedometer tests. A sensitivity analysis was conducted to explore the influence of contact model parameters on the sample preparation and the shear stage of triaxial tests. The influence of parameters like rolling resistance friction coefficient, inter-particle friction coefficient, effective modulus, and normal-to-shear stiffness ratio were investigated. For calibration of the DEM model, the input parameters were selected such that the simulations reproduce the macro mechanical characteristics like dilation angle, peak stress, and stiffness. The calibrated parameters were then validated by simulating a one-dimensional compression test. The results are in good agreement with the experiments, which proves the suitability of the calibrated parameters. In addition, the validated parameters were applied to investigate the mechanical behaviour including the evolution of contact force chains, non-coaxiality of principal stress and strain rate, and sample inhomogeneity during a simple shear test.

Keywords: Distinct element method; rolling resistance linear; calibration; oedometer; triaxial; simple shear.

1. Introduction

Granular materials are ubiquitous in daily life and their engineering behaviour is controlled by their particulate nature. At the particle level, characteristics like shape, size, gradation, and at the meso-scale, force chain evolution and fabric (e.g. contact orientations) determine the mechanical response of granular materials. For such materials, physical modelling using homogeneous and isotropic continuum-based methods cannot entirely capture the intricate micro and mesoscale interactions which control the macro scale behaviour. The Distinct Element Method (DEM) can address the particulate nature of granular material. However, the quality of such simulations depend on the contact model parameters. The parameter calibration is more of an optimisation problem termed as the bulk calibration approach, where the simulated macro response is matched to an experimental macro response under similar boundary conditions (Boikov et al. 2018). It has been reported that selecting a unique set of parameters that can be used to simulate loading paths different from those used for calibration is a challenge that has not been addressed yet (Sibille et al. 2019).

It is widely accepted that the mode of shear within a shear band and in grounds under seismic shear loading is simple shear. The rotation of principal stress axes during progressive shearing has been reported by Oda and Konishi (1974) and the amount of principal stress and strain rotation, the intermediate principal stress variation, the orientation of the failure surface, and stress and strain nonuniformity inside the specimen have been the subject of much discussion (Asadzadeh and Soroush 2016). The evolution of the internal stresses as well as the soil fabric cannot be easily captured in the laboratory. Here, DEM acts as an aid to experiments to analyse microscale behaviours.

DEM has been used by many researchers to simulate simple shear tests for granular materials. Shi et al. (2015) simulated the simple shear behaviour of dense granular assemblies using 2D simulations and reported that the non-coaxiality decreases with strain level and that the rotation of the principal direction of fabric anisotropy lags behind that of major principal stress direction during simple shear. Guitterez and Muftah (2015) examined the evolution of force chains, buckling of columns of particles, particle rolling and formation of voids within the shear band using 2D DEM simulations. The authors reported high degrees of particle rotation and large voids within the localised shear band during the simple shear mode of deformation. Dabeet et al. (2015) investigated the non-uniformities of stresses and strains of a simulated direct simple shear (DSS) experiment. The response of glass bead specimens simulated with the boundary conditions of three variations of simple shear devices namely stacked-ring, Cambridge and NGI types were investigated by Asadzadeh and Soroush (2016). The authors reported that the direction of principal stress rotates towards that of the principal strain rate, gradually

reducing the degree of non-coaxiality from about 45° to fluctuating around 0°. The rate of approaching coaxiality is slower in samples with larger initial porosity, stress ratio, and mean stress (Ai et al. 2014). Li et al. (2020) modelled an NGI Type bidirectional simple shear apparatus with clumps as boundaries, which can be moved by particles within the specimen. The present study aims at calibrating the input parameters for the rolling resistance linear model and validating the input parameters based on one- dimensional compression tests. Further, simple shear experiment is simulated and the response is analysed. The study is part of a comprehensive research aimed at analysing the behaviour at the soil-structure interface.

2. Methodology for calibration and validation of the DEM model

The basic formulation for the DEM is described in Cundall and Strack (1979). The contact forces and the accelerations are determined through a series of calculations tracing the particle movements. Newton's second law is used to determine the motion of each particle arising from the contact and body forces acting upon it, while the force-displacement law is used to update the contact forces arising from the relative motion at each contact. Using these incremental displacements and rotations, the particle positions and orientations are updated. Spherical particles are widely used to model granular materials and offer the advantage that it allows easier contact detection, thus reducing simulation time. However, in reality, the grains are not spherical and possess surface asperities, which contribute to the phenomenon of "interlocking" that influences the macro mechanical response of granular materials. Rolling resistance contact models have gained popularity with the introduction of a rolling resistance moment, which adds resistance at the contacts to particles rotation. The present study utilises spherical particles and the rolling resistance linear model based on the Iwashita and Oda (1998) model implemented in the commercial software Particle Flow Code 3D to model the particle interactions.

2.1. Calibration of contact parameters through triaxial tests

The sand investigated in the present study is glacial Quartz sand from Cuxhaven, north Germany, termed "Cuxhaven sand" henceforth where numerous wind power plants are in operation. The grain size distribution and an image captured through a laser microscope is found in Figure 1. The mean values of roundness and sphericity as per Krumbein und Sloss (1963) is 0.54 and 0.77 respectively. The significant classifying parameters of the sand are listed in Table 1.

As a first step, three-dimensional true triaxial simulations were conducted to calibrate the rolling resistance linear contact model parameters of Cuxhaven sand. Around 10,000 spherical particles were created within a cubical sample of size 5mm such that a high target porosity was reached. The spherical particle or balls were distributed within the container such that the size distribution matched the grain size distribution obtained in the laboratory. A comparison can be found in Figure 1. A polyaxial cell consisting of planar walls that form a rectangular cuboid was created to provide the rigid boundary condition for a true triaxial test. The wall elements were used to confine the sample. A linear contact model was applied at the grain-wall contact and the ball-facet friction was set to zero. The boundary contraction method as described in the material modelling support package of PFC3D was used to create samples of initial relative density similar to that of the experiment (refer Table 2). A cloud of grains was created and allowed to rearrange into a packed state until zero mean stress is achieved with zero inter-particle friction.

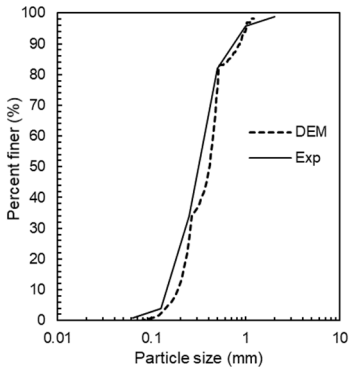

(a)

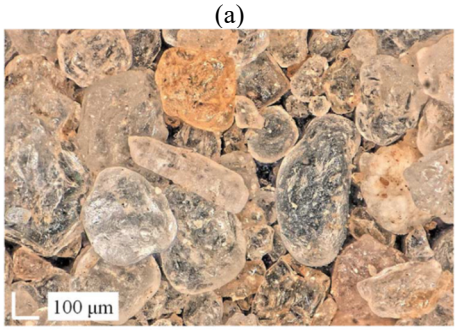

(b)

Figure 1. Grain size distribution curve through experiment and from simulated sample and (b) image of Cuxhaven sand captured through a confocal laser microscope (Bock, et al. 2021)

Table 1. Physical properties of Cuxhaven sand

Mean size d_{50} [mm]	Specific gravity ρ_s [g/cm^3]	Maximum void ratio e_{max} [-]	Minimum void ratio e_{min} [-]
0.30	2.65	0.75	0.48

The large overlaps were reduced during this phase until an overlap ratio of 0.25 was reached. Then an inter-particle friction coefficient μ was set to attain a particular void ratio and confinement was applied by moving the walls under servo-control until the pressures of all servo-controlled walls were within a tolerance of 0.01. The configuration of the triaxial sample after boundary contraction can be found in Figure 2. The determination of the relative density D_r of the simulated sample for calibration with the real granular material is quite challenging. Many researchers have created simulated samples at void ratio values similar to laboratory samples. However, this approach is questionable as the maximum and minimum void ratio achieved for a

simulated sample composed of spheres are largely different from the experiment due to the different particle shapes in experiments and simulations. In the present study, the limiting void ratios were simulated by setting the coefficient μ to 0 and 0.5.

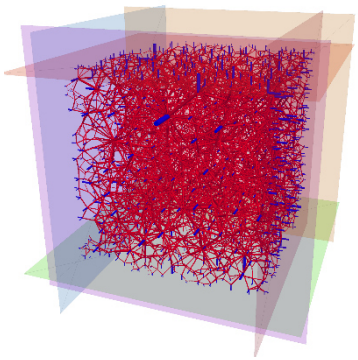

Figure 2. Contacts between particles of the simulated triaxial sample after boundary contraction

Once the initial states were simulated, a sensitivity analysis was conducted to identify the effect of the intrinsic parameter of effective modulus E^*, inter-particle friction coefficient μ, rolling resistance friction coefficient μ_r on the initial void ratio and mechanical response of the simulated sample. During this process, other intrinsic parameters like normal-to-shear stiffness ratio k_{rat} and damping coefficient were kept constant. It was observed that the introduction of coefficient μ_r is important to achieve the loosest state. The rolling resistance friction coefficient μ_r was kept constant at 0.5 to identify the influence of μ, which influences the simulation of denser states. The influence of isotropic stress applied during boundary contraction is minor in comparison to the other factors. The coefficients μ and μ_r are kept constant at 0.5 to analyse the influence of effective modulus E^* on the initial void ratio achieved. It was observed that a specimen with lower E^* can be compacted to a denser state. The parameters used to achieve the limiting void ratio and void ratios corresponding to relative densities of 40%, 90% under isotropic stress state are listed in Table 2.

The sample was sheared after the required initial relative densities were achieved. The velocity during shear was limited such that the inertial number was small enough to enforce a quasi-static state. The samples were sheared till an axial strain of 20% is reached. During the shear phase, the intrinsic parameters E^*, k_{rat} and contact parameters μ, μ_r were varied to calibrate the contact model parameters. The calibration of contact model parameters with the triaxial experimental results is conducted for a relative density of 90% subjected to isotropic stress of 300kPa. The calibration is carried out such that the macroscopic parameters like peak friction angle, critical state friction angle, Poisson's ratio, and dilation angle are similar to the experiment.

It was observed that higher values of k_{rat} results in higher peak deviator stress values. However, the effect is limited at axial strains higher than 10%. The effective modulus E^*affects the stress response of the specimen within the elastic range. The initial slope of stress-strain response increases sharply with increasing effective modulus. However, the influence of E^*on peak stress and critical stress is not significant.

Table 2. Relative densities achieved by varying inter-particle friction coefficient μ

μ	Void ratio e (-)	Relative density D_r (%)
0.00	0.48	100.00
0.10	0.55	90.00
0.23	0.65	40.00
0.50	0.79	0.00

The coefficient μ should be adjusted to achieve a dilation angle and peak stress similar to the experiments. The coefficient μ was selected as 0.42, which resulted in a match between the peak stress in the model and the experiment. The coefficient $\mu_r$is affected by the particle shape, normal stiffness, and normal force at a point of contact and typically ranges from 0 to 1 (Gutierrez and Muftah 2015). However, Huang et al. (2014) found that after exceeding certain value, μ_r has little influence on the response at specific values of μ.

The procedure of parameter calibration adopted in the present study can be summarized as follows. In the first step, the modulus $E^*$is selected according to the initial slope of stress-strain behaviour "the elastic range". Then k_{rat} should be selected based on the comparison between simulations and experimental data. The coefficient μ_r influences the response within the range of 0.1-0.4. The influence becomes less significant if $\mu_r > 0.4$. The selection of coefficient μ has to be done before μ_r to approach the dilation behavior as close as possible. Then, the coefficient μ_r is lowered to adjust the peak stress behaviour. The calibrated input parameters of the rolling resistance linear model are listed in Table 3.

Table 3. Calibrated parameters of rolling resistance linear model

Parameter		Value
Effective modulus (MPa)	E^*	700.00
Normal-to-shear stiffness ratio	k_{rat}	5.00
Inter-particle friction coefficient	μ	0.42
Rolling resistance friction coefficient	μ_r	0.36

As an initial means of validation, the calibrated input parameters were then used to simulate a triaxial test at a lower relative density of 40%. The calibrated parameters are used to simulate shear behaviour under triaxial conditions under relative densities of 40 and 90% and under confining stresses of 150 and 300kPa. The stresses and strains were calculated from the walls. The evolution of the deviator stress vs axial strain is depicted in Figure 3(a) and Figure 4(a). Figure 3(b) and Figure 4(b) show the corresponding volumetric vs axial strain response. In Figure 3(a) it can be seen that the modelled deviator stress and axial strain behaviour are in good agreement with that in the experiment. Furthermore, the peak deviator stress is attained at an axial strain of around 4%. The stress response at larger axial strains is similar in a qualitative and quantitative manner.

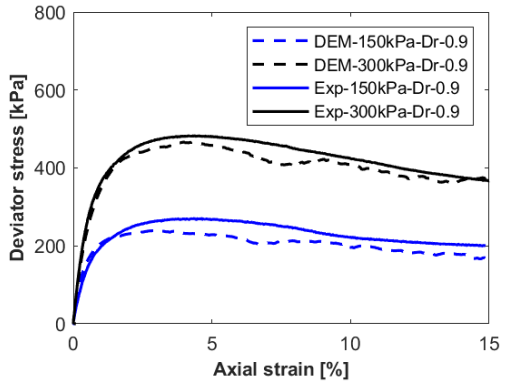

(a)

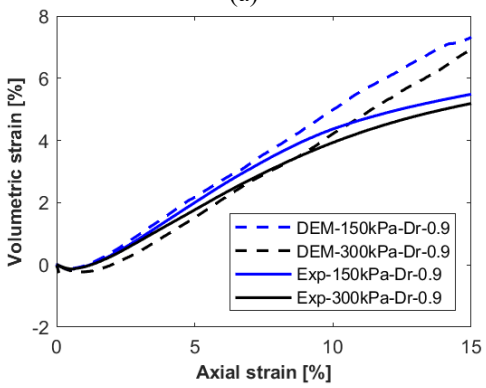

(b)

Figure 3. Comparison between (a) deviator stresses vs axial strain (b) volumetric strain vs axial strain obtained from experimental and simulated triaxial tests on Cuxhaven sand at a relative density of 0.9

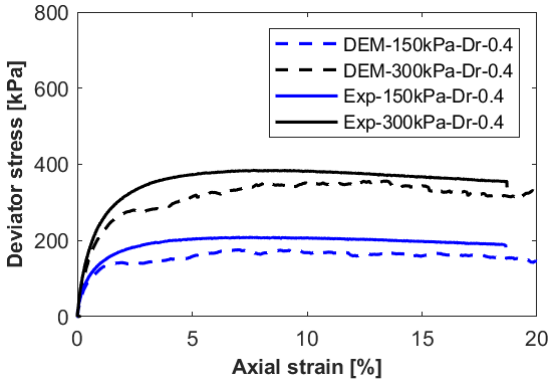

(a)

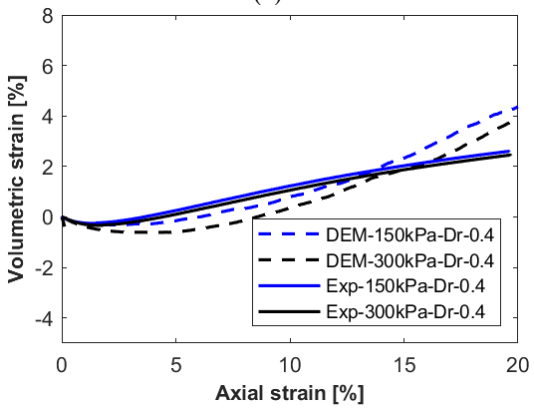

(b)

Figure 4. Comparison between (a) deviator stresses vs axial strain (b) volumetric strain vs axial strain obtained from experimental and simulated triaxial tests on Cuxhaven sand at a relative density of 0.4

It can be observed from Figure 3(b) that the Poisson's ratio and dilatancy angle are similar till an axial strain of 10%, indicating a similar volumetric response. From Figure 3, it can be concluded that the simulation is in reasonable agreement in terms of the shear and the volumetric response of the dense sample at two confining stresses. It can be observed that the simulated response for medium dense samples in Figure 4 (a) and (b) matches the experimental data to a limited extent when compared to the dense samples. The change from contractant to dilatant behaviour in the simulation happens at an axial strain of 5% whereas it occurs at an axial strain of 1% in the experiment. The trend of the shear response and the volumetric behaviour were captured in a fairly good agreement through the calibrated parameters.

2.2. Validation of contact model through oedometer test

The feasibility of the calibrated set of parameters is justified by applying them to validate the results of a one-dimensional oedometric compression test. The simulated oedometer sample is cylindrical with a diameter of 100mm and an initial height of 30mm similar to the experiment. The bottom and sidewalls were constrained in all directions during the sample generation and compression stages. The top wall moves in the vertical direction to achieve the desired axial stress. The axial stress was calculated by averaging the total contact force of the top wall and bottom wall. The generation of particles and simulation of relative densities were similar to the procedure explained above. The coefficient μ was set to 0.15 to create a sample with a relative density of around 70% as in the oedometer experiment.

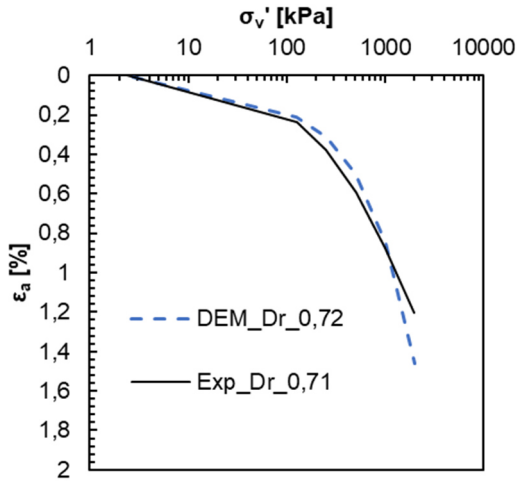

Figure 5. Oedometric compression curves from experiment and DEM simulation of cuxhaven sand at a relative density of 0.7

All parameters calibrated from the triaxial test were built into the rolling resistance linear contact model to simulate the behaviour of Cuxhaven sand under one-dimensional compression. The sample was compressed axially and the axial strain was continuously monitored and is plotted in Figure 5. Each loading phase was cycled until the stresses achieved the tolerance limit of 0.01 and the average unbalanced force ratio is less than 0.001. It is

clear from Fig. 5, that the simulation can predict the one-dimensional compression behaviour to a moderate extent. Considering the difficulty of the validation of the model using complex loading paths as mentioned in Sibille et al. (2019), the trend of the compression curve predicted by the simulation fits the experimental curve.

3. Forecast of behavior of Cuxhaven sand under simple shear

The calibrated and validated input parameters were then used to forecast the behaviour of Cuxhaven sand under simple shear. The specimen was cylindrical with a diameter of 70 mm and a height of approximately 28.6 mm. This diameter-to-height ratio agrees with the recommendations by Franke (1979), which minimizes the non-uniformities during shearing.

In the simple shear test, each laminar confining ring was modelled as a wall group, comprising two short vertical cylindrical walls and two cones that serve as the horizontal connection between the cylindrical walls. The sample was contained within 10 rings as seen in Figure 6. All rings were fixed in $z-$axis while being free in xy-plane. Bernhardt (2016) conducted simulations with 35 thin confining rings and proved that the vertical thickness has limited effects on the results. Particles were formed within the container with overlaps such that the gradation matches the experimental grain size distribution. The particles were scaled 5 times, resulting in around 30,000 balls. The overlap ratio was calculated as the quotient of the contact gap and radius of the balls and the particles were rearranged until an overlap ratio of less than 0.25 was reached.

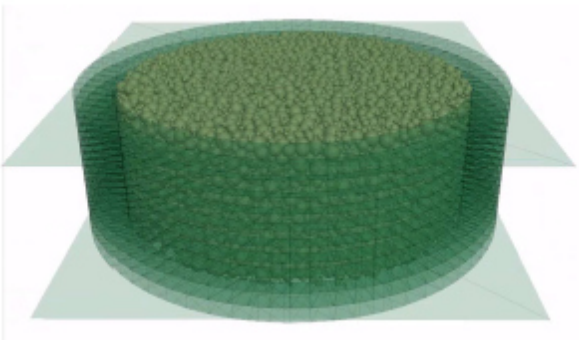

Figure 6. Simulated simple shear cell with confining rings

To account for the friction between the membrane and sand in the experiment, a ball-facet friction coefficient of 0.1 was used in this study. The ball-facet contact stiffness was set to a value of 1.5e9 Pa since Li et al. (2020) suggest a stiffness around 2-3 times bigger than that of balls. After overlap reduction and contact model assignment, the specimen was ready to be compacted and sheared. An isotropic stress was applied to the sample by means of vertical and radial stress on the walls. The radial stress was obtained by iterating all the contact forces on the side cylindrical walls and dividing it with the contact area.

A vertical force was applied on the top wall to apply a stress of 200kPa. The simulations were conducted at velocities that were sufficiently small to ensure quasi-static conditions. The velocity during the shear phase was set to 0.2mm/min. The shear phase was accomplished by applying linearly increased velocities in x direction to the rings from top to bottom. The top wall and its adjacent ring were fixed and the velocity of the second ring from the top was 1/9 x velocity, that of the third ring was 2/9*velocity and so on until the velocity of the last ring and the bottom plate was the actual velocity. During the shearing process, the stress state was documented for shear strain values of 5%, 10%, 15% and 20% to analyse the results.

3.1. Results

The contact force network can be used to show the distribution of microscale contacts and transmission of contact forces. Figure 7 shows the top view (xz-plane), front view (xy-plane) of contact force chains in the 3D DEM model. The thickness of the lines is proportional to the magnitude of contact forces and the orientation denotes the direction of contact normal. From the contact force chains on the left in Figure 7 (a) and (b), it can be seen that the contact forces are rather randomly orientated after consolidation. Some boundary effects (inhomogeneity) are observed. After 10% shear strain, contact force chains slightly incline diagonally towards the direction of induced shear strains. At the end of the shearing at an axial strain of 20%, the strong contact forces (darker and wider lines) are remarkably concentrated along the dominant shear direction. For instance, the strong contact forces projected on the xz plane approach a notable diagonal distribution and the contact forces in other directions get weaker, similar to the distribution under unidirectional shear conditions obtained by Thornton and Zhang (2006) and Asadzadeh and Soroush (2016).

Following Huang et al. (2014), the homogeneity of the samples at the initial state and during shearing was examined to gain some understanding of the influence of the particle-to-sample size ratio on the observed response. As reported by Bernardt et al. (2016), the packing density in the top vertical boundary and the inhomogeneity across the vertical direction of the sample play more important roles in terms of influencing the stress-strain and volumetric differences. In this work, homogeneity was quantified vertically by dividing the sample into 6 zones, which were approximately 4.6 mm thick respectively (refer Figure 8). The zone thickness was selected to always exceed the largest particle diameter. The void ratio in each zone e_{zone} is calculated dividing the total void volume in each zone (difference between total volume of balls and the volume of each zone) by the sum of volume of all particles in the corresponding zone. The normalized void ratio calculated as a ratio of void ratio of the zone e_{zone} and the total void ratio e_{tot} of the whole specimen at 0%, 10%, and 20% shear strain is shown in Figure 8. The legend shows that lighter colour gradation has lower normalised void ratios, whereas darker colour indicates larger normalised void ratios. Referring to Figure 8, there are large variations in the void ratio distribution in the vertical axis for all strain ranges. The void ratio at the bottommost layer exceeds the total void ratio by approximately 31% during shearing. A similar effect is

noted in the topmost layer, however, it is not as loose as the bottom layer exceeding the total void ratio by 8%. In addition to large diameter-to-height ratios, the number of particles represented within the core of the element is also important (Bernhardt et al. 2016). In the case of a simple shear element where the height of the sample is the limiting dimension, it is critical that a sufficient number of particles be represented across the height of the sample.

When shear localisation occurs within a sample, the particle rotations occur extensively within the shear band. Shear localisation in the simple shear test has been evaluated by analysing the orientation of four columns of particles represented in Figure 9(a). The location of the columns of particles at a shear strain of 40% is shown in Figure 9(b). Since there is no obvious buckling of columns, it can be concluded that either no shear band has developed during shear at 40% shear strain, which might be due to the low coefficient μ_r or that the entire sample is localised. Shear localisation was reported by Gutierrez and Muftah (2014) in a 2D simple shear DEM simulation running up to 50% shear strain, in which a higher rolling resistance coefficient of 0.5 was used. A higher rolling resistance coefficient increases the bending stiffness of a column and, at the same time, increases the instability related to buckling. A lower rolling resistance coefficient allows the particle to move more freely and is more unlikely to form a column due to lack of rigidity. Li et al. (2020) simulated Leighton Buzzard sand, a sub rounded particle, using a rolling resistance coefficient of 0.2 and observed no obvious buckling.

Another important aspect regarding simple shear tests as pointed out by Hill (1950) is non-coaxiality, which is an important aspect of material anisotropy. Coaxiality, which refers to the coincidence of principal directions of stress and inelastic incremental strain, is a fundamental assumption of classical flow theory (Qian et al. 2008).

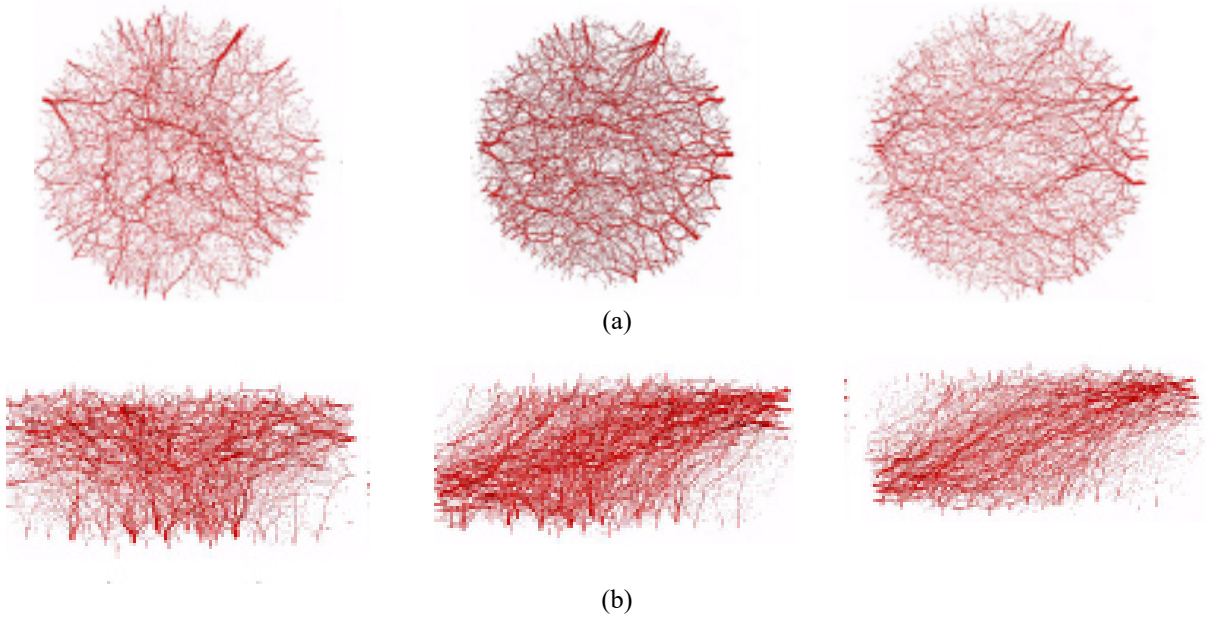

Figure 7. Contact force chains developed during simple shear test (a) top view (b) front view. The left, middle and right pictures show the force chains before shear, at shear strain of 10% and shear strain of 20% respectively.

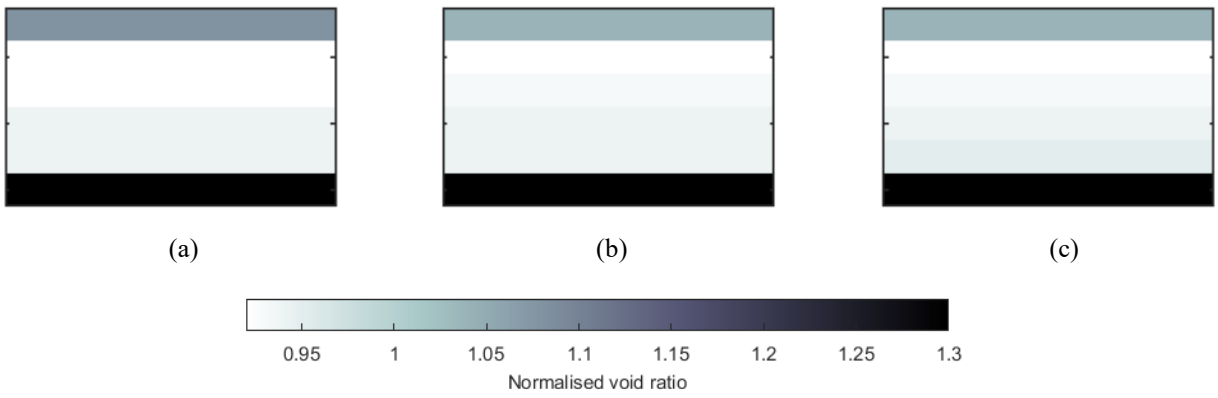

Figure 8. Normalised void ratio distribution along sample height and total void ratio etot at shear strains of (a) 0% (b) 10% (c) 20%.The corresponding total void ratios are 0.587; 0.575 and 0.576

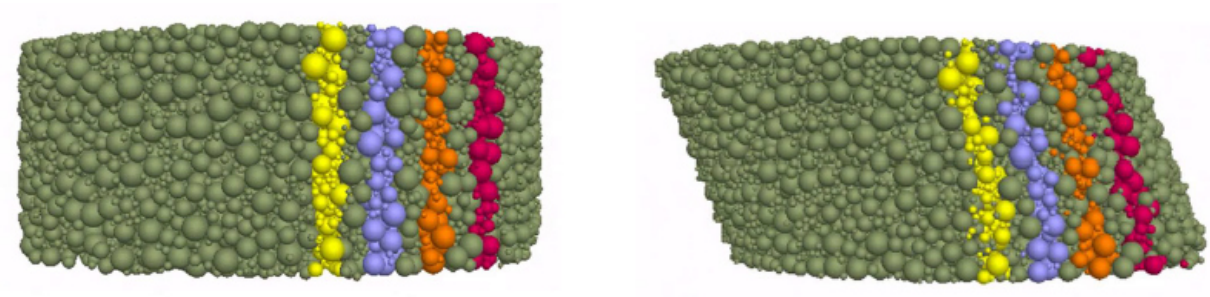

(a) (b)

Figure 9. Column of particles created to identify shear localisation (a) before shear (b) after shear till 20%

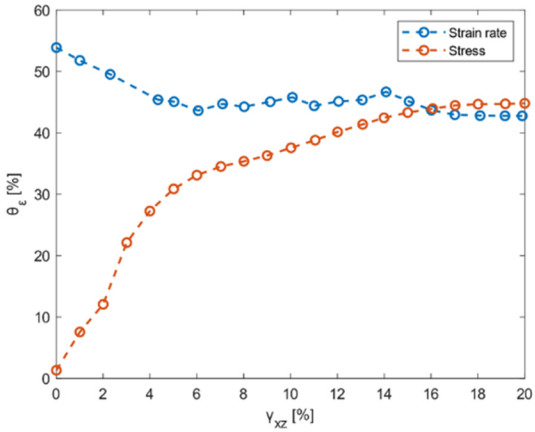

Figure 10. The change of principal orientation angles of stress and strain rate with increasing strain during simple shear

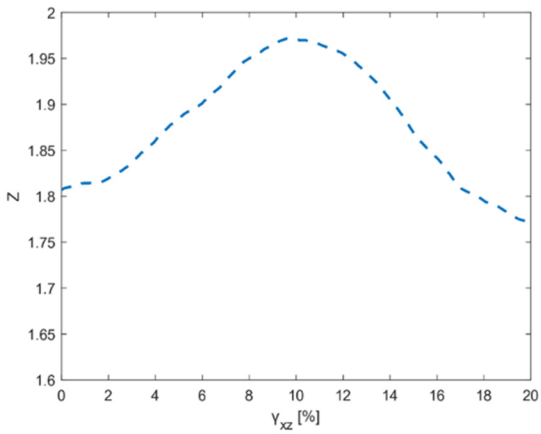

Figure 11. Development of coordination number Z with increasing shear strain during simple shear

In contrast, the principal orientation angle of the strain rate is varying near 45°. The unusually unstable and high angle in the first phase may result from the measurement sphere chosen. It can be concluded that the degree of non-coaxiality is the greatest at the beginning of shear. When the shear strain reaches around 15%, the degree of non-coaxiality is already close to 0. This result is similar to previous studies conducted by Qian, Huang and Sun (2011).

The coordination number Z is used to describe the packing intensity, which is an important characteristic of the material fabric. It is defined as the average number of active contacts per particle within the granular material. The coordination number in Figure 11 increases with the contraction of the granular assembly and decreases with the assemblies' dilation. The coordination number just after the consolidation is 1.81. From shear strain 0% to around 13%, the coordination number increased from 1.81 to 1.97 indicating contractive behaviour and the highest contact density. After reaching peak point, the packing density keeps decreasing to 1.77, which shows a dilative response and lower contact density. Thus, the coordination number associated with the volumetric change indicates the relation between macro-scale deformation and microscale structure.

4. Conclusions

In this study, the DEM model parameters for the rolling resistance linear model for Cuxhaven sand were calibrated and validated through triaxial and oedometer tests. The calibrated parameters are used to forecast the behaviour of Cuxhaven sand under simple shear boundary conditions. The parameters are mainly calibrated by trial-and -error process. The parameters are interdependent and hence this process is time intensive. However, in this present study, a guideline on the influences of different input parameters is outlined. The minimum and maximum void ratios required to calculate the relative density are achieved by adjusting the inter-particle friction coefficient during sample generation. The effective modulus is set to align the deviator stress behaviour within the "elastic range" to the experiments. Then the normal-to-shear stiffness ratio is adjusted through a trial-and-error process to deal with the volumetric behaviour. When the volumetric strain behaviour is in good agreement with experiments, the inter-particle and rolling resistance friction coefficient are adjusted to approach the peak deviator stress. The set of parameters calibrated following this approach proves to be reasonable to simulate triaxial tests and oedometer test and is hence used to forecast simple shear behaviour. The evolution of contact force chains vividly shows the distribution of the strong contact network. The inhomogeneity of void ratios along the sample height is calculated and documented throughout the shearing phase, which shows looser structures in the top and bottom layers. Shear localisation is not observed likely due to the small rolling resistance coefficient. The non-coaxiality of principle stress and strain rate is also well captured. The changes in coordination number indicate

the contact density and volumetric response. The degree of non-coaxiality is greatest at the beginning of shear and decreases as the sample is being sheared. While DEM has limitations on the number of particles and difficulty in accurately defining some material response, it still has been able to provide valuable insight into the microscopic behaviour that otherwise would be unavailable. Further shear test simulations incorporating the real particle shape are being conducted. The parameters calibrated as part of the study are valid only for the rolling resistance linear contact model and will need to be calibrated again if considering non-spherical grains with clumps or rigid blocks. Future work will also focus on investigating the interface behaviour on soil-structure interaction problems and its dependency on particle level scale.

Acknowledgements

The authors are grateful for the support provided by Itasca Consulting Group through its Itasca Educational Partnership (IEP) Teaching Program for the use of the PFC 3D software.

References

Ai, J., P.A. Langston, and H.S. Yu. 2014 "Discrete element modelling of material non-coaxiality in simple shear flows." International Journal for numerical and analytical methods in geomechanics: 615-635. https://doi.org/10.1002/nag.2230

Asadzadeh, M., and A. Soroush. 2016 "Fundamental investigation of constant stress simple shear test using DEM." Powder Technology 292: 129-139. https://doi.org/10.1016/j.powtec.2016.01.029

Bernhardt, M., G. Biscontin, and C. O'Sullivan. 2016 "Experimental validation of 3D direct simple shear DEM simulations." Soils and Foundations: 336-347. https://doi.org/10.1016/j.sandf.2016.04.002

Bock, B.A., F. Levin, S. Vogt, and R. Cudmani. 2021 "Acoustic emission of sand during creep under oedometric compression." Geotechnical Testing Journal. https://doi.org/10.1520/GTJ20210007

Boikov, A.V., R.V. Savelev, and V.A. Payor. 2018 "DEM Calibration approach: design of experiment." International Conference Information Technologies in Business and Industry. https://doi.org/10.1088/1742-6596/1015/3/032017

Cundall, P.A., and O.D. Strack. 1979 "A discrete numerical model for granular assemblies." Géotechnique 29(1): 47-65. https://doi.org/10.1680/geot.1979.29.1.47

Dabeet, A., D. Wijewickreme, and P. Byrne. 2015 "Evaluation of stress strain non-uniformities in the laboratory direct simple shear test specimens using 3D discrete element analysis." Geomechanics and Geoengineering. https://doi.org/10.1080/17486025.2014.979889

Franke, E.K. 1979 "A new direct simple shear test device." Geotechnical Testing Journal. https://doi.org/10.1520/GTJ10457J

Gutierrez, M., and A. Muftah. 2014 "Micro-mechanical observations of strain localization in granular soils during simple shear loading." Bifurcation and degradation of geomaterials in the new millennium: 27-32. https://doi.org/10.1007/978-3-319-13506-9_5

Hill, R. 1950 The mathematical theory of plasticity.

Huang, X., K.J. Hanley, C. O'Sullivan, and F.C.Y. Kwok. 2014 "Effect of sample size on the response of DEM samples with a relaistic grading." Particuology, Volume 15: 107-115. https://doi.org/10.1016/j.partic.2013.07.006

Iwashita, K., and M. Oda. 1998 "Rolling Resistance at Contacts in Simulation of Shear Band Development by DEM." Journal of Engineering Mechanics ASCE 124. https://doi.org/10.1061/(ASCE)0733-9399(1998)124:3(285)

Krumbein, W., and L.L. Sloss. 1963 Stratigraphy and sedimentation. San Franscisco: Freeman.

Li, Y., P. Su, and Z. Wang. 2020 "Improved boundary conditions for a 3D DEM simple shear model." Advances in civil engineering. https://doi.org/10.1155/2020/5420793

Oda, M., and J. Konishi. 1974 "Rotation of principal stresses in granular material during simple shear." Soils and Foundations: 39-53. https://doi.org/10.3208/sandf1972.14.4_39

Qian, J., M. Huang, and H. Sun. 2011 "Macro-mechanical approaches for non-coaxiality of coarse grained soils." Science China Technological Sciences, Vol. 54: 147-153. https://doi.org/10.1007/s11431-011-4634-3

Qian, J.G., J. Yang, and M.S. Huang. 2008 "Three-dimensional noncoaxial plasticity modeling of shear band formation in geomaterials." Journal of engineering mechanics, https://doi.org/10.1061/(ASCE)0733-9399(2008)134:4(322)

Shi, D., J. Xue, Z. Zhao, and J. Shi. 2015 "A DEM investigation on simple shear behaviour of dense granular assemblies." Journal of Central South University: 4844-4855. https://doi.org/10.1007/s11771-015-3036-2

Sibille, L., P. Villard, F. Darve, and R.A. Hosn. 2019 "Quantitative prediction of discrete element models on complex loading paths." International Journal for Numerical and Analytical methods in geomechanics: 858-887. https://doi.org/10.1002/nag.2911

Thornton, C., and L. Zhang. 2006 "A numerical examination of shear banding and simple shear non-coaxial flow rules." Philosophical Magazine: 3425-3452. https://doi.org/10.1080/14786430500197868

Zhang, M., Y. Yang, H. Zhang, and H. Yu. 2019 "DEM and experimental study of bi-directional simple shear." Granular matter: 21-24.